Scientia Iranica B (2015) 22(2), 467–486

Sharif University of Technology
Scientia Iranica
Transactions B: Mechanical Engineering
www.scientiairanica.com

On dynamic non-prehensile manipulation of multibody objects

B. Beigzadeh[a,*] and A. Meghdari[b]

a. *School of Mechanical Engineering, Iran University of Science and Technology, Narmak, Tehran, P.O. Box 16846-13114, Iran.*
b. *Center of Excellence in Design, Robotics, and Automation (CEDRA), Department of Mechanical Engineering, Sharif University of Technology, Tehran, Iran.*

Received 25 January 2014; received in revised form 29 June 2014; accepted 18 August 2014

KEYWORDS
Dynamic manipulation;
Object manipulation;
Multibody objects;
Robotics;
Systems with impulse effects.

Abstract. In this paper, we construct a framework for studying dynamic non-prehensile manipulation systems during which multi-link manipulators can manipulate multibody objects. The multibody object is multilink, with some actuators in the joints, which complicates the manipulation process, because the control of the object configuration cannot be decoupled from the control problem of the whole process. The manipulation problem includes a series of similar manipulators manipulating a multibody object. Both the object and the individual manipulator can be fully actuated, under actuated, or passive. The object has two contact surfaces that are in alternate contact with the manipulator contact surface. Each manipulator carries the object during a contact phase and passes it to the next manipulator. The passing of the object from one manipulator to another is an instantaneous phase, namely the impact phase. Therefore, the whole process is a nonlinear process with impulse effects.

After deriving a formulation for the general problem, we solve three representative examples to show the concept. In these examples, we study the manipulation of active and passive objects using active and passive manipulators. Dynamics, control, motion planning and orbital stability during the presence of impact are the most important challenges in this work.

1. Introduction

Dynamic manipulation of objects is a challenging and important branch of robotics, and is an evolutionary form of traditional manipulation. In traditional manipulation, the manipulation is done by grasping objects and then manipulating them. However, in dynamic manipulation, we use the dynamic behavior of the object to manipulate it. Dynamic Non-prehensile Manipulation (DNM), however, may cover a wide variety of dynamic manipulation problems, like the work introduced in this paper. Non-prehensile manipulation refers to a kind of manipulation without a form or force-closure grasp. Using DNM, it is possible to manipulate an object too large or heavy to be grasped and lifted by eliminating the gripper. Therefore, the structure of the manipulator is simplified. DNM allows a manipulator to control multiple parts simultaneously, using whatever surfaces of the manipulator are available. If we define the workspace of a robot as the set of reachable states for an object manipulated by the robot, the size of the robot's workspace is effectively increased by throwing the object to points outside the robot's kinematic workspace [1]. In this work, not only do we take advantage of the dynamic behavior of an

*. *Corresponding author. Tel.: +98 21 77240094; Fax: +98 21 73021587*
E-mail addresses: b_beigzadeh@iust.ac.ir (B. Beigzadeh); meghdari@sharif.edu (A. Meghdari)

object in regard to manipulation, but also apply some controlled actions to the object's actuator to control and improve its dynamic behavior in such a way that the manipulation process becomes more stable. This way it is possible to manipulate objects with more complicated structures.

DNM covers a wide range of problems in robotics. Beigzadeh et al. [2] dynamically manipulated a disc by throwing and catching it using two planar manipulators, while the disc had an angular velocity. In [3], Beigzadeh et al. undertook a kind of dynamic object manipulation, during which a series of three-link manipulators dynamically manipulated a polygonal object by catching it from the previous manipulator and passing it on to the next. Akbarimajd et al. undertook kinematical modeling and planning for the problem of dynamic manipulation of objects using a series of one DOF manipulators [4]. Other examples of DNM include planning for the manipulation of polygonal objects using 1 DOF manipulators [5], quasi-static manipulation, such as pushing with point contact [6], or pushing parts on a conveyor belt with a one joint part feeder [7], dynamic manipulation of active objects [8], control and manipulation of multibody objects [9], and manipulation of multibody active objects, using simple passive manipulators [10].

In this work, we study both active and passive systems. Most of the aforementioned work could be categorized as including active systems. However, if no actuators are employed in the manipulation system, the resulting system is passive. Passive dynamic object manipulation was first introduced by Beigzadeh et al. in [11] and later in [12]. Most passive robotic systems are passive walkers. Some work undertaken in this direction and related to this aspect of the current study includes actuating a simple 3D passive dynamic walker [13] and studying the passive turning in 3D compass gait walkers [14].

This work can be categorized as a dynamical system with impulse effects. Stability issues regarding these nonlinear systems, including orbital stability of the periodic solutions of autonomous systems, have been explored in [15]. Hurmuzlu et al. offered mathematical models to study the effect of impact in mechanical bipedal locomotion systems [16]. Then, they studied the structural stability of these discontinuous systems via a perturbation method and analysis of the phase-plane portraits of the generalized coordinates [17]. In the same manner, Grizzle et al. designed a feedback control for systems with impulse effects, i.e. bipedal locomotion systems, and proved that their system would have an asymptotically stable limit cycle [18-19]. Although the basis of the stability analysis used in the current study comes from this mentioned work, it is not in the same class of robotics. This work is a pioneer in studying the dynamic manipulation of active objects with periodic behavior.

1.1. Motivation and outlines

This work is part of an extensive study to analyze the correlation of bipedal locomotion and dynamic object manipulation. An abstract view of this idea was published in [20]. We are interested in defining an integrated system, whose special cases include bipedal locomotion systems.

Let us consider an object manipulated by a manipulator, dynamically, i.e. without any static grasp. If the object is not rigid, e.g. multibody objects, we should derive its dynamic equation of motion so that its dynamic behavior is predictable. If the object has enough (m) actuators to change and control its configuration, the problem of manipulation becomes more solvable. However, the problem of object control will be added to the manipulation problem.

We have focused on the manipulation of active multibody objects using a series of manipulators. However, this focus can be clustered into sub problems of manipulating the objects using two manipulators. In this study, the object should be passed from one manipulator to the other. It is clear, in this case, that impact occurrence is inevitable. Impact occurrence complicates the problem, because the presence of impulse effects in a nonlinear dynamical system means that we have a hybrid periodic system whose stable behavior will need the thorough study and analysis of stabilizer control methods. Here, we deal with such a problem.

In this paper, a simple model of an object is assumed to be manipulated. The object is a mass with two active arms playing the role of contact surfaces during the manipulation process. Moreover, one DOF manipulators are used to manipulate the active object. At the end of the manipulator, a flat surface is considered as a contact surface and touches the contact surfaces of the object during the manipulation process.

The whole manipulation problem is divided into sequential cycles, each of which consists of two separate phases. For each phase, we offer the dynamic model of the system, including those of both object and manipulators. Some conditions are derived, so that satisfying them guarantees the local stability of the process. In this way, a new point, namely, PRI, is introduced to check non-relative rotating conditions regarding the object.

For control of the system in each cycle, we use input-output linearization and the concept of zero dynamics, which is known in nonlinear control. Afterward, a special case of feedback control, which has been introduced in [21], is applied for zeroing the outputs in order to achieve zero dynamics. The overall stability of the whole process is taken into account using the

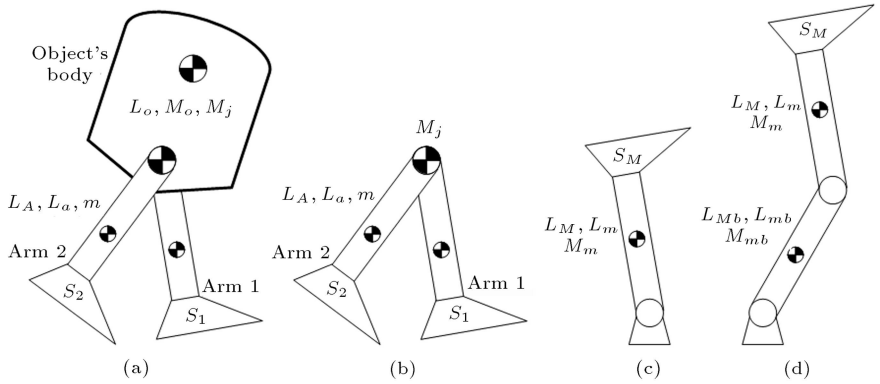

Figure 1. Different types of multibody object and manipulator and corresponding parameters: (a) Multibody three-segment object including body and two arms, and S_1 and S_2 as contact surfaces; (b) multibody two-link object including only two arms, and S_1 and S_2 as contact surfaces; (c) simple one-link manipulator with flattened end-effector S_M as contact surface; and (d) two-link manipulator with flattened end-effector, S_M, as contact surface.

analysis of the Poincare map. Finally, simulations support the results.

2. Modeling and planning

The problem discussed here is a kind of dynamic manipulation process. In this process, we use a series of planar m-link manipulators (here, $m = 1, 2$, as in Figure 1(c) and (d)) to manipulate multibody n-link objects (here, $n = 2, 3$, as in Figure 1(a) and (b)). Each manipulator, the kth manipulator, may have an actuator in every joint, and has a flattened end-effector, S_M, S_M^k, which plays the role of the contact surface during manipulation. Moreover, we simply assume that each kind of object has two arms as the contact surfaces, namely, S_1 and S_2 (Figure 1(a) and (b)). These arms will be alternatively in contact with the manipulator end-effector during the manipulation process. Furthermore, we assume that the objects could be active objects. An active object has enough actuators in its joints to be capable of controlling its own shape. Here, we study the manipulation of both active and passive multibody objects, using both fully actuated and under-actuated manipulators.

During manipulation, by our definition, the cycle, k, is a part of the manipulation process which starts at time τ_k, with the impact of one arm, with the end-effector of manipulator k, and finishes at time τ_{k+1}, with the impact of the other arm, with the end-effector of manipulator $k+1$. More precisely, a cycle begins just before one impact, and ends just before the next. Therefore, each cycle can be divided into two separate phases with no overlap: *Impact Phase* and *Contact Phase*. The manipulation process is then a series of such cycles.

2.1. Contact phase

In this study, we assume that the whole process is a sequence of alternate contact and impact phases. Every contact phase results in an impact phase. The duration of the impact phase is very short (as we expect from mechanical systems) and changes the states of the system. Then, the new states are the initial conditions for the next contact phase. In fact, the manipulation process is wholly a contact phase with some impulse effects. The contact phase is then defined when arm 1 is in contact with end-effector k ($k = 1, 2, 3, \cdots$). That is, S_1 lies exactly on S_M^k with no slippage or separation. By this assumption, it is reasonable to consider that the sliding joint between contact surfaces acts as a fixed joint and, therefore, we may assume that arm 1 and end-effector k are a united part in a new object-manipulator system during the successful cycle, k.

To write a dynamic equation for each m-link manipulator, we need m generalized coordinates, while $n+2$ generalized coordinates are needed for a free n-link object. Therefore, $m + n + 2$ generalized coordinates are needed for dynamic equations of the whole system. However, in the new object-manipulator system, we only need $m + n - 1$ generalized coordinates to write the dynamic equations of motion. That is, the absolute orientation and Cartesian coordinates of arm 1 equal those of end-effector k, which means that it is not necessary to define these three coordinates separately. When designing a controller and undertaking path-planning for the system, we will take into account that no slippage and separation conditions should be satisfied in the whole process. Then, for such a system, with an n-link object and an m-link manipulator, the governing dynamic equation for the contact phase is:

$$\mathbf{M}(\mathbf{q})\ddot{\mathbf{q}} + \mathbf{C}(\mathbf{q}, \dot{\mathbf{q}})\dot{\mathbf{q}} + \mathbf{G}(\mathbf{q}) = \mathbf{B}\mathbf{u},$$

$$\mathbf{y} = h(\mathbf{q}, \dot{\mathbf{q}}), \tag{1}$$

where $\mathbf{q} \in \mathbb{R}^{n+m-1}$, $\mathbf{M}$ and $\mathbf{C}$ are, respectively, $m + n - 1$ square matrices, and $\mathbf{G}$, $\mathbf{u} \in \mathbb{R}^{n+m-1}$.

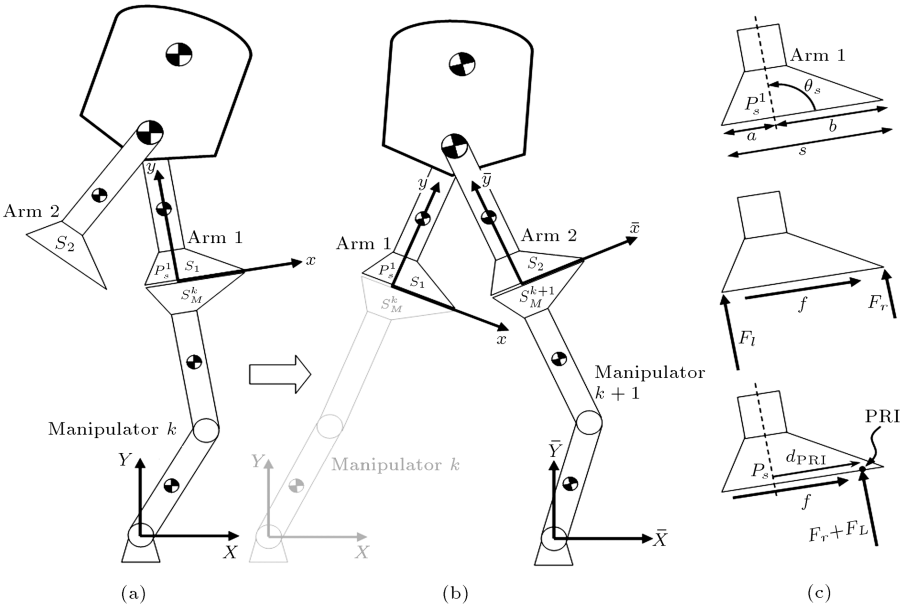

Figure 2. Schematic view of contact phase k and impact phase $k+1$: (a) Contact phase k: contact surfaces, absolute and local coordinates; (b) impact phase $k+1$: contact surfaces, absolute and local coordinates. The object collides with manipulator $k+1$ and leaves manipulator k carrying the object during the previous cycle; and (c) contact surface of arm 1, its parameters, dimensions, forces acting on it during contact phase, PRI point and its relative distance from P_s^1. These parameters are similar to those of the impact phase, i.e. corresponding definitions are the same.

To avoid the probable slippage and separation of arm 1 from end-effector k, we derive some mathematical conditions corresponding to these two events. We notice that contact surfaces cannot grasp or pull each other. This means that only compressive forces, and not tensional forces, are allowable between them. Therefore, the normal contact forces between them can be only compressive. In addition, the direction of the whole contact reaction force should be in the friction cone to ensure that no slippage occurs during the contact phase. To check the validity of these conditions, we should compute the mentioned reaction forces. As the manipulator bases are fixed, we assume that the inertial frame, $X-Y$, is attached to the base point of manipulator, k, during contact phase, k (see Figure 2(a)). Then, for a given trajectory, it is possible to write the position of the object's center of mass, $\mathbf{P}_O^{\mathrm{CM}}$, as a function of $\mathbf{q}$, $\Psi(\mathbf{q})$. So, for its velocity and acceleration, $\mathbf{v}_O^{\mathrm{CM}}$and $\mathbf{a}_O^{\mathrm{CM}}$, we have:

$$\mathbf{v}_O^{\mathrm{CM}} = \frac{\partial \Psi(\mathbf{q})}{\partial \mathbf{q}}\dot{\mathbf{q}}, \tag{2}$$

$$\mathbf{a}_O^{\mathrm{CM}} = \frac{\partial}{\partial \mathbf{q}}\left(\frac{\partial \Psi(\mathbf{q})}{\partial \mathbf{q}}\dot{\mathbf{q}}\right)\dot{\mathbf{q}} + \frac{\partial \Psi(\mathbf{q})}{\partial \mathbf{q}}\ddot{\mathbf{q}}. \tag{3}$$

Then. we may simply write:

$$\mathbf{F}_c^1 = m_{\mathrm{total}}\mathbf{R}(\mathbf{a}_O^{\mathrm{CM}} - \mathbf{g}), \tag{4}$$

where $\mathbf{R}$ maps $\mathbf{a}_O^{\mathrm{CM}}$ from the inertial frame to the local frame, $x-y$, attached to the end-effector, k (see Figure 2(a)). It is noted that the effect point of $\mathbf{F}_c^1$ is P_s^1, which is simply the intersection of the contact surface direction and the line connecting the last joint of manipulator, k, and the first joint of arm 1 (see Figure 2(a) and (c)). Because we assume that the contact surfaces compose a fixed joint, there is a couple acting on S_1, in addition to $\mathbf{F}_c^1$, namely, $\mathbf{M}_c^1$, which must be determined. Having written the equation of momentum of the system about the manipulator base, and rearranged the terms, we obtain:

$$\mathbf{M}_c^1 = \dot{\mathbf{H}} - \mathbf{P}_s^1 \times \mathbf{R}^T\mathbf{F}_c^1. \tag{5}$$

We model this virtual couple by dividing the y-element of $\mathbf{F}_c^1$ into two parallel forces, F_l and F_r, and imposing these forces on the left and right edges of S_1, respectively (see Figure 2(c)). The other component of $\mathbf{F}_c^1$ (which is parallel to S_1), that is, f, is due to frictional effects. With a little investigation, we may write:

$$f = \mathbf{F}_c^1.\mathbf{e}_x, \tag{6}$$

$$F_r = \frac{a\mathbf{F}_c^1.\mathbf{e}_y + \mathbf{M}_c^1}{a+b}, \tag{7}$$

$$F_l = \frac{b\mathbf{F}_c^1.\mathbf{e}_y - \mathbf{M}_c^1}{a+b}. \tag{8}$$

Having obtained the unknowns, f, F_r and F_L, we should check the validity of the following inequalities to ensure that the contact surface, S_1, neither slips nor

separates from S_M^k:

$$F_l, F_r \geq 0, \tag{9}$$

$$\frac{|f|}{|F_l + F_r|} < \mu_s. \tag{10}$$

An equivalent analysis can also be taken into account. First, we notice that the contact surface, S_M^k, cannot exert actual torque to S_1 by grasping. So, we model it by moving the effect-point of $\mathbf{F}_c^1$ along S_1, and search for a point where no torque acts on S_1. Conceptually, such a point is the same as the FRI (Foot-Rotation Indicator) point in walking robots [22]. We may call this new point the PRI (Palm-Rotation Indicator) point, as it indicates whether the palm of the object would rotate with respect to the contact surface, S_M^k [23]. In fact, the point on the contact surface, S_1, where the net reaction force of the manipulator acts without any torque, is the PRI point. Its distance from P_s^1 can be obtained from:

$$d_{\text{PRI}} = \frac{\mathbf{M}_c^1.\mathbf{e}_z}{\mathbf{F}_c^1.\mathbf{e}_y}. \tag{11}$$

Then the analysis says that Conditions (9) and (10) become:

$$\mathbf{F}_c^1.\mathbf{e}_y > 0, \tag{12}$$

$$-a < d_{\text{PRI}} < b, \tag{13}$$

$$\frac{|f|}{|\mathbf{F}_c^1.\mathbf{e}_y|} < \mu_s. \tag{14}$$

Eq. (12) clarifies that the contact surface, S_M^k, cannot grasp S_1. Eq. (13) indicates that the PRI point must be inside S_1 to avoid contact surface S_1 from rotating, with respect to the S_M^k.

2.2. Impact phase

In a successful manipulation, when the system is in the kth contact phase, arm 1 is in contact with S_M^k corresponding to the manipulator, k. Thus, time reaches τ_{k+1} and the contact phase ends by reaching impact $k+1$. Then free arm 2 collides with the end-effector, $k+1$. An impact phase is successful if no slip or rebound occurs between S_2 and S_M^{k+1} corresponding to the manipulator, $k+1$, during impact, while arm 1 lifts off the end-effector, k, simultaneously. This is the end of impact phase $k+1$ and the beginning of contact phase $k+1$. We assume that the impact phase is instantaneous, and interaction forces are impulsive in this phase. Therefore, only velocities experience some instantaneous changes while positions are continuous and unchanged. In addition, it is assumed that the actuators cannot produce impulsive responses.

An exact impact model is described in [24] and used later in [18]. We use a similar approach with some modifications. For the analysis of the system during the impact phase, we assume the object and the manipulator, $k+1$, to be a united system. Therefore, we analyze this new system during impact. As there might be impulse reactions in the contact surfaces and manipulator base during impact, we should consider these impulses in our dynamic equations as net forces. Thus, the dynamic equation of the system is:

$$\mathbf{M}(\mathbf{q}_i)\ddot{\mathbf{q}}_i + \mathbf{C}(\mathbf{q}_i, \dot{\mathbf{q}}_i)\dot{\mathbf{q}}_i + \mathbf{G}(\mathbf{q}_i) = \mathbf{B}\mathbf{u} + \mathbf{J}^T\mathbf{F}_{\text{ext}}, \tag{15}$$

where $\mathbf{q}_i$ includes generalized coordinates of the object and manipulator $k+1$. So, its dimension is $n+m+4$; the object has $n-1$ body coordinates, the manipulator has $m-1$ body coordinates, the two coordinates are for inertial orientation of both object and manipulator, and the remaining four coordinates are Cartesian coordinates of any point of the object and manipulator. By integrating Eq. (15) during the impact phase, with respect to time $t \in (\tau_{k+1}^-, \tau_{k+1}^+)$, where signs (-) and (+) refer to just before and just after impact, and noting that $\mathbf{q}_i^+ = \mathbf{q}_i^- = \mathbf{q}_i$, we may have:

$$\mathbf{M}(\mathbf{q}_i)(\dot{\mathbf{q}}_i^+ - \dot{\mathbf{q}}_i^-) = \mathbf{J}^T\hat{\mathbf{F}}_{\text{ext}}, \tag{16}$$

where:

$$\hat{\mathbf{F}}_{\text{ext}} = \int_{\tau_{k+1}^-}^{\tau_{k+1}^+} \mathbf{F}_{\text{ext}}\, dt. \tag{17}$$

In this equation, $\mathbf{q}_i$ and $\dot{\mathbf{q}}_i^-$ are known from the previous contact phase by defining two pre-transition functions, $\bar{\Delta}_V$ and $\bar{\Delta}_P$, that is:

$$\mathbf{q}_i = \bar{\Delta}_P(\mathbf{q}^-), \tag{18}$$

$$\dot{\mathbf{q}}_i^- = \bar{\Delta}_V(\dot{\mathbf{q}}^-). \tag{19}$$

In these equations, $\mathbf{q}^-$ and $\dot{\mathbf{q}}^-$ include variables of the object and the manipulator, k, while $\mathbf{q}_i$ and $\dot{\mathbf{q}}_i^-$ contain positions and velocities of the object and the manipulator, $k+1$. Afterward, we note that $\dot{\mathbf{q}}_i^+$ and $\hat{\mathbf{F}}_{\text{ext}}$ are unknowns in Eq. (16) and should be determined. We need some other equations to find the unknowns. No rebound condition results in plastic impact, that is:

$$\epsilon = 0. \tag{20}$$

The no-slip condition, however, forces the contact surfaces, S_2 and S_M^{k+1}, to have no relative velocity just after impact. In other words, these conditions impose three constraints onto the system during impact:

$$(V_s^2)_x^+ = (V_M^{k+1})_x^+, \tag{21}$$

$$(V_s^2)_y^+ = (V_M^{k+1})_y^+, \tag{22}$$

$$(\theta_s^2)^+ = (\theta_M^{k+1})^+. \tag{23}$$

Constraints (21) and (22) mean that point P_s^2 adheres to P_M^{k+1}, while Constraint (23) says that arm 2 and end-effector $k+1$ have the same angular velocity after impact. We may impose these constraints onto the system to obtain a new definition of the impact problem. As in the contact phase, we suppose that the object and manipulator are an integrated system. Constraints (21) and (22) suggest that the Cartesian position of the manipulator can be defined as a position of P_M^{k+1}. When in the impact phase, it coincides with P_s^2. In addition, the absolute orientation of the manipulator can be defined by the absolute orientation of the end effector, which is equal to the absolute orientation of arm 2 (refer to Condition (23)). Therefore, the dimension of $\mathbf{q}_i$ is reduced to $n+m+1$. Then, it includes the body coordinates of both object and manipulator, absolute orientation of some link of either the manipulator or the object, and Cartesian coordinates of a point of either. Also, in this definition, $\hat{\mathbf{F}}_{\text{ext}}$ only includes impulse reactions on the manipulator base and contact surface, S_1. Also, we may conclude that there is no impulse reaction acting on the contact surface, S_1 [24]. To show this, we say that if there is any impulse reaction, we may write:

$$\Delta V^+_{S_1/S_M} + \epsilon.\Delta V^-_{S_1/S_M} = 0. \tag{24}$$

On the other hand, from the contact phase, we know that:

$$\Delta V^-_{S_1/S_M} = 0. \tag{25}$$

No matter the value of ϵ, substituting Eq. (25) in Eq. (24) results in:

$$\Delta V^+_{S_1/S_M} = 0. \tag{26}$$

It is not possible in our problem, because, as we discussed before, in the impact phase, free arm 2 collides with end-effector $k+1$, while arm 1 lifts off end-effector k, simultaneously. Therefore, it is necessary to have:

$$\Delta V^+_{S_1/S_M} \neq 0, \tag{27}$$

which is in contrast to Eq. (26). Thus, we conclude that there is no impulse reaction between S_1 and S_M^k corresponding to manipulator k. This means that $\hat{\mathbf{F}}_{\text{ext}}$ only includes impulse reactions acting on the base of manipulator $k+1$.

We note that the left-hand side of Eq. (16) is, in fact, the change of system momentum, $\mathbf{\Sigma}$, due to impulse $\hat{\mathbf{F}}_{\text{ext}}$. That is:

$$\mathbf{\Sigma}_{\text{after}} - \mathbf{\Sigma}_{\text{before}} = \mathbf{J}^T \hat{\mathbf{F}}_{\text{ext}}, \tag{28}$$

where:

$$\mathbf{\Sigma}_{\text{after}} = \mathbf{M}(\mathbf{q}_i)\dot{\mathbf{q}}_i^+, \tag{29}$$

and:

$$\mathbf{\Sigma}_{\text{before}} = (\mathbf{M}(\mathbf{q}_i) - \mathbf{M}_{S_M}(\mathbf{q}_i))\dot{\mathbf{q}}_i^-. \tag{30}$$

In Eq. (30), $\mathbf{M}_{S_M}(\mathbf{q}_i)\dot{\mathbf{q}}_i^-$ is the virtual momentum added to $\mathbf{M}(\mathbf{q}_i)\dot{\mathbf{q}}_i^-$, due to considering arm 2 and end effector $k+1$ as one segment, while end effector $k+1$ is motionless before impact. Therefore, no momentum corresponding to this segment should be included in $\mathbf{\Sigma}_{\text{before}}$. Thus, in Eq. (30), we subtract virtual momentum $\mathbf{M}_{S_M}(\mathbf{q}_i)\dot{\mathbf{q}}_i^-$ from $\mathbf{M}(\mathbf{q}_i)\dot{\mathbf{q}}_i^-$, where:

$$K_{S_M}(\mathbf{q}_i, \dot{\mathbf{q}}_i^-) = \frac{1}{2}\left(\dot{\mathbf{q}}_i^T\right)^- \mathbf{M}_{S_M}(\mathbf{q}_i)\dot{\mathbf{q}}_i^-. \tag{31}$$

And $K_{S_M}(\mathbf{q}_i, \dot{\mathbf{q}}_i^-)$ is the virtual kinetic energy of end effector $k+1$, due to the assumption of its adhering to arm 1 just before impact.

In addition, we note that the base of manipulator $k+1$, where impulse reaction $\hat{\mathbf{F}}_{\text{ext}}$ is acting, is fixed, and, thus, we may write:

$$\mathbf{J}\dot{\mathbf{q}}_i^+ = 0_{2\times 2}. \tag{32}$$

Combining Eqs. (28)-(30), and (32) results in:

$$\begin{bmatrix} \mathbf{M} & -\mathbf{J}^T \\ \mathbf{J} & 0_{2\times 2} \end{bmatrix} \begin{bmatrix} \dot{\mathbf{q}}_i^+ \\ \hat{\mathbf{F}}_{\text{ext}} \end{bmatrix} = \begin{bmatrix} (\mathbf{M} - \mathbf{M}_{S_M})\dot{\mathbf{q}}_i^- \\ 0_{2\times 1} \end{bmatrix}. \tag{33}$$

After solving Eq. (33) for unknowns, we have:

$$\begin{bmatrix} \dot{\mathbf{q}}_i^+ \\ \hat{\mathbf{F}}_{\text{ext}} \end{bmatrix} = \begin{bmatrix} \mathbf{M} & -\mathbf{J}^T \\ \mathbf{J} & 0_{2\times 2} \end{bmatrix}^{-1} \begin{bmatrix} (\mathbf{M} - \mathbf{M}_{S_M})\dot{\mathbf{q}}_i^- \\ 0_{2\times 1} \end{bmatrix}. \tag{34}$$

Or:

$$\begin{bmatrix} \dot{\mathbf{q}}_i^+ \\ \hat{\mathbf{F}}_{\text{ext}} \end{bmatrix} = \begin{bmatrix} \mathbf{M}^{-1} - \mathbf{M}^{-1}\mathbf{J}^T(\mathbf{J}\mathbf{M}^{-1}\mathbf{J}^T)^{-1}\mathbf{J}\mathbf{M}^{-1} & \mathbf{M}^{-1}\mathbf{J}^T(\mathbf{J}\mathbf{M}^{-1}\mathbf{J}^T)^{-1} \\ (\mathbf{J}\mathbf{M}^{-1}\mathbf{J}^T)^{-1}\mathbf{J}\mathbf{M}^{-1} & (\mathbf{J}\mathbf{M}^{-1}\mathbf{J}^T)^{-1} \end{bmatrix} \times \begin{bmatrix} (\mathbf{M} - \mathbf{M}_{S_M})\dot{\mathbf{q}}_i^- \\ 0_{2\times 1} \end{bmatrix}, \tag{35}$$

which gives us a relation for $\dot{\mathbf{q}}_i^+$ as:

$$\dot{\mathbf{q}}_i^+ = \Delta_V(\mathbf{q}_i, \dot{\mathbf{q}}_i^-), \tag{36}$$

where:

$$\Delta_P(\mathbf{q}_i, \dot{\mathbf{q}}_i^-) = \mathbf{M}^{-1} - \mathbf{M}^{-1}\mathbf{J}^T(\mathbf{J}\mathbf{M}^{-1}\mathbf{J}^T)^{-1}\mathbf{J}\mathbf{M}^{-1}(\mathbf{M} - \mathbf{M}_{S_M})\dot{\mathbf{q}}_i^-. \tag{37}$$

We want the system to satisfy the no rebound and no slip condition during impact. To check the validity of these conditions, we should compute the contact reaction impulses. During the impact phase, it is possible to write the position of $\mathbf{P}_O^{\mathrm{CM}}$ as a function of $\mathbf{q}_i$ and $\bar{\Psi}(\mathbf{q}_i)$. So, we may simply write:

$$\hat{\mathbf{F}}_c^2 = m_{\mathrm{total}}\bar{\mathbf{R}}^- \frac{\partial\bar{\Psi}(\mathbf{q}_i)}{\partial\mathbf{q}_i}(\dot{\mathbf{q}}_i^+ - \dot{\mathbf{q}}_i^-), \tag{38}$$

where $\bar{\mathbf{R}}$ maps any Cartesian vector from the inertial frame to the local frame, $\bar{x}-\bar{y}$, attached to the end-effector, $k+1$ (see Figure 1(b)). Then, by integrating Eq. (5) during impact, we have:

$$\hat{\mathbf{M}}_c^2 = \mathbf{H}^+ - \mathbf{H}^- - \mathbf{P}_s^2 \times \left(\bar{\mathbf{R}}^-\right)^T \hat{\mathbf{F}}_c^2. \tag{39}$$

Afterwards, corresponding to Relations (6)-(8), we have three relations as:

$$\hat{f} = \hat{\mathbf{F}}_c^2.\mathbf{e}_{\bar{x}}, \tag{40}$$

$$\hat{F}_r = \frac{a\hat{\mathbf{F}}_c^2.\mathbf{e}_{\bar{y}} + \hat{\mathbf{M}}_c^2.\mathbf{e}_{\bar{z}}}{a+b}, \tag{41}$$

$$\hat{F}_l = \frac{b\hat{\mathbf{F}}_c^2.\mathbf{e}_{\bar{y}} - \hat{\mathbf{M}}_c^2.\mathbf{e}_{\bar{z}}}{a+b}. \tag{42}$$

Then, the no rebound and no slip conditions get mathematical forms as:

$$\hat{F}_l, \hat{F}_r \geq 0, \tag{43}$$

$$\frac{\left|\hat{f}\right|}{\left|\hat{F}_l + \hat{F}_r\right|} < \mu_s. \tag{44}$$

As in the contact phase, it is possible to rewrite Relations (43) and (44) by analyzing the PRI point in the impact phase. Again, d_{PRI}, which is defined in Eq. (11) and equals the distance of PRI from P_s^2 on S_2, is computed as:

$$d_{\mathrm{PRI}} = \frac{\hat{\mathbf{M}}_c^2.\mathbf{e}_{\bar{z}}}{\hat{\mathbf{F}}_c^2.\mathbf{e}_{\bar{y}}}. \tag{45}$$

Here, PRI is the point on contact surface S_2 where the net impulse reaction force of manipulator $k+1$ acts on S_2 without any impulse torque. Therefore, no rebound and no slip conditions are:

$$\hat{\mathbf{F}}_c^2.\mathbf{e}_{\bar{y}} > 0, \tag{46}$$

$$-a < d_{\mathrm{PRI}} < b, \tag{47}$$

$$\frac{|f|}{\left|\hat{\mathbf{F}}_c^2.\mathbf{e}_{\bar{y}}\right|} < \mu_s. \tag{48}$$

Another condition to be taken into account is the separation of arm 1 from manipulator k. This could be checked by calculating the linear velocities of the left and right edges of S_1, and determining whether these points separate from the corresponding points on the manipulator. As we discussed before, there is no impulse reaction, on S_1. Therefore, manipulator k does not experience any change in its velocities during the impact phase. This means that the post-impact velocities of the contact surface of manipulator k equal its velocities just before impact, and, therefore, are equal to the velocities corresponding to S_1 just before impact. That is, we only need to focus on the linear and angular velocities of S_1 just before and just after impact. Considering that the Cartesian coordinate of the systems contributing to $\mathbf{q}_i$ corresponds to the P_s^1 on S_1, we may easily extract the pre- and post-impact velocities from $\mathbf{x}^-$ and $\mathbf{x}^+$ obtained from Eqs. (36) and (37). Now, the conditions assuring us that S_1 separates from S_M^k of manipulator k are:

$$\mathbf{R}^T\left(\left(\mathbf{V}_s^1\right)^+ - \left(\mathbf{V}_s^1\right)^-\right).\mathbf{e}_y + b\left(\left(\dot{\theta}_s^1\right)^+ - \left(\dot{\theta}_s^1\right)^-\right) > 0, \tag{49}$$

$$\mathbf{R}^T\left(\left(\mathbf{V}_s^1\right)^+ - \left(\mathbf{V}_s^1\right)^-\right).\mathbf{e}_y - a\left(\left(\dot{\theta}_s^1\right)^+ - \left(\dot{\theta}_s^1\right)^-\right) > 0. \tag{50}$$

Having checked Conditions (49) and (50), along with Conditions (43) and (44), or (46), (47), and (48), we rename arm 1, arm 2 and the local and global coordinates in such a way that arm 1 is in contact with end-effector $k+1$; arm 2 is free, and other variables are the same as in the previous contact phase. The whole transition process can be completed simply by using some transition functions, namely Δ_P and Δ_V, that is:

$$\mathbf{q}^+ = \Delta_P\left(\mathbf{q}_i^-\right), \tag{51}$$

$$\dot{\mathbf{q}}^+ = \Delta_V\left(\dot{\mathbf{q}}_i^-\right). \tag{52}$$

Eqs. (51) and (52) imply that we have some switching mechanism in the whole process, which makes our system hybrid. In fact, we are dealing with a nonlinear dynamic system with impulse effects.

2.3. State space and hybrid model

By defining state variable $\mathbf{x}$ as:

$$\mathbf{x} = \left[\mathbf{q}^T, \dot{\mathbf{q}}^T\right]^T, \tag{53}$$

dynamic model (1) for the contact phase can be written as:

$$\dot{\mathbf{x}} = f(\mathbf{x}) + g(\mathbf{x})\mathbf{u},$$
$$\mathbf{y} = h(\mathbf{x}), \tag{54}$$

where:

$$f(\mathbf{x}) = \begin{bmatrix} \dot{\mathbf{q}} \\ -\mathbf{M}^{-1}\left(\mathbf{C}\dot{\mathbf{q}} + \mathbf{G}\right) \end{bmatrix}, \tag{55}$$

$$g(\mathbf{x}) = \mathbf{M}^{-1}\mathbf{B}. \tag{56}$$

Then, using Eqs. (18) and (19), transition models (51) and (52) will be:

$$\mathbf{x}^{+} = \begin{bmatrix} \Delta_P \circ \bar{\Delta}_P\left(\mathbf{q}^{-}\right) \\ \Delta_V \circ \bar{\Delta}_V\left(\dot{\mathbf{q}}^{-}\right) \end{bmatrix} = \Delta\left(\mathbf{x}^{-}\right). \tag{57}$$

It is important to note that when the contact phase reaches state $\mathbf{x}^{-}$, impact occurs and transition model (57) should be applied to compute the $\mathbf{x}^{+}$ as a new initial state for the next contact phase. In fact, we have a nonlinear dynamic system with an impulse effect that is defined as:

$$\begin{aligned} &\dot{\mathbf{x}} = f(\mathbf{x}) + g(\mathbf{x})\mathbf{u} && \mathbf{x} \notin S, \\ &\mathbf{x} = \Delta(\mathbf{x}) && \mathbf{x} \in S, \end{aligned} \tag{58}$$

where:

$$S = \left\{ \mathbf{x} \,|E(\mathbf{x}) = 0, \mathbf{q} \in (0, 2\pi)^{n+m-1}, \dot{\mathbf{q}} \in \mathbb{R}^{n+m-1} \right\}. \tag{59}$$

And $E(\mathbf{x})$ is any function of $\mathbf{q}$, whose vanishing indicates the reaching of arm 1 to the end-effector $k+1$, e.g. the distance between them.

3. Control and stability

In this paper, we deal with three categories of manipulation systems:

I. Dynamic manipulation of active objects using active manipulators;

II. Dynamic manipulation of under-actuated objects using active manipulators;

III. Dynamic manipulation of active objects using under-actuated manipulators.

The integrated object/manipulator system in the first category is a fully actuated system, while it is under-actuated in the others. The control strategies used in under-actuated systems are usually different from those applied to fully actuated systems. We can then use a single approach of postural control with some minor differences. Therefore, we first design for an appropriate output function, y in Eq. (54), which is a function of $\mathbf{q}$ only. Due to the second order nature of the model, the first time-derivative of $\mathbf{y}$ does not explicitly depend on $\mathbf{u}$. It is the second time-derivative, which includes $\ddot{\mathbf{q}}$, that shows a direct relation between $\ddot{\mathbf{y}}$ and $\mathbf{u}$. Therefore, the relative degree of $\mathbf{y}$ is two. Consequently, by direct calculation, we have:

$$\ddot{\mathbf{y}} = \mathcal{L}_f^2 h\left(\mathbf{q}, \dot{\mathbf{q}}\right) + \mathcal{L}_g \mathcal{L}_f h(\mathbf{q})\mathbf{u}. \tag{60}$$

The decoupling matrix, $\mathcal{L}_g \mathcal{L}_f h(\mathbf{q})$, depends only on $\mathbf{q}$ and determines the controllability of the system. If it is invertible in its domain of definition, applying the feedback control:

$$\mathbf{u} = \left(\mathcal{L}_g \mathcal{L}_f h(\mathbf{q})\right)^{-1}\left(\mathbf{v} - \mathcal{L}_f^2 h\left(\mathbf{q}, \dot{\mathbf{q}}\right)\right), \tag{61}$$

results in:

$$\ddot{\mathbf{y}} = \mathbf{v}. \tag{62}$$

There are several possibilities for $\mathbf{v}$ so wherein $\mathbf{y}$ is driven to zero. However, for the sake of the stability of the system, we need $\mathbf{y}$ to equal zero before the contact phase intersects S defined in Eq. (59). Therefore, we should search for a control which makes the origin of Eq. (62) finite-time stable. One possible option is the controller proposed in [15], which is defined for a double integrator system:

$$\ddot{x} = v, \tag{63}$$

with $v \in \mathbb{R}$. Then, the feedback:

$$v = \psi\left(x, \dot{x}, \alpha_1, \alpha_2\right) = -|x|^{\alpha_1}\text{sign}(x) - |\dot{x}|^{\alpha_2}\,\text{sign}\left(\dot{x}\right), \tag{64}$$

where $\alpha_2 \in (0, 1)$ and $\alpha_1 > \alpha_2/(2-\alpha_2)$ makes the origin of Eq. (63) globally finite-time stable, and its settling time depends continuously on the initial condition. Applying this controller to System (62) results in a control action of the form:

$$\begin{aligned} \mathbf{u} = -\left(\mathcal{L}_g \mathcal{L}_f h(\mathbf{x})\right)^{-1}\left(|\mathbf{x}|^{\alpha_1}\text{sign}(\mathbf{x})\right. \\ \left. + |\dot{\mathbf{x}}|^{\alpha_2}\,\text{sign}\left(\dot{\mathbf{x}}\right) + \mathcal{L}_f^2 h(\mathbf{x})\right). \end{aligned} \tag{65}$$

To check the stability of the system, we define an appropriate Poincare map and search for its fixed point. Then, we determine whether it is asymptotically stable. Let us consider $\mathbf{y}$ in Eq. (54) as:

$$\mathbf{y} = h(\mathbf{x}) = h_a(\mathbf{q}) - h_d(\gamma(\mathbf{q})). \tag{66}$$

It is notable that the number of constraints we may impose onto the system is, at most, equal to the number of system actuators. That is, for a system with one degree of under-actuation, for example, we could control the shape of the system only and not the absolute orientation of the whole system.

The feedback (65) makes $h_a(\mathbf{q})$ identical, being equal to $h_d(\gamma(\mathbf{q}))$ in finite time. Also, $\gamma(\mathbf{q})$ can be chosen in such a way that it reflects the absolute orientation of the system in some way. As we cannot directly control the change of $\gamma(\mathbf{q})$, it helps us to analyze the stability of the system. Now, if $\gamma(\mathbf{q})$ has a stable limit cycle, we may expect each of the system's outputs to have a stable periodic behavior. This can guarantee the stability of the whole system.

In the case of successful manipulation, Eq. (65) assures us that the object has reached the end-effector (the system intersects S) in an appropriate configuration. That is, at the moment of impact, $\gamma(\mathbf{q}^-)$ is known. However, $\dot{\gamma}(\mathbf{q}^-, \dot{\mathbf{q}}^-)$ may vary depending on the stability condition of the system. An appropriate Poincare section may be defined just before impact. An option for a one-dimensional Poincare map is $\kappa(\dot{\gamma}^-)$, which maps $\dot{\gamma}^-$ just before impact onto the $\dot{\gamma}^-$, just before the next impact, that is:

$$\dot{\gamma}^-_{k+1} = \kappa(\dot{\gamma}^-_k). \tag{67}$$

By starting from $\dot{\gamma}^-_k$ and assuming that at impact k, $\mathbf{y}$ is zero, $\mathbf{q}^-$ can be easily computed; if the controller properly forces $\mathbf{y}$ to be zero before each impact, $\mathbf{q}^-$ is unchanged during manipulation. With the aid of the same assumption, we can compute $\dot{\mathbf{q}}^-$ for any $\dot{\gamma}^-_k$. Then, applying Eq. (57) gives us $\mathbf{x}^+$, which can be used as the initial condition of the contact phase model (54) or (58). Model (58) should be solved until it intersects S. If $\mathbf{y}$ has been forced to equal zero, then, $\dot{\gamma}^-_{k+1}$ is the output of the function, κ and $\dot{\gamma}^-_k$ is a valid point in its domain of definition. The intersection of the diagram of κ for its domain of definition with the identity line is the fixed point of κ and, of course, of the system. At this point, if the slope of the diagram is less than 1, it is an asymptotically stable fixed point. If the slope is more than 1, it is unstable and, in the case where the slope equals 1, the fixed point is semistable [17]. Figure 3 shows four possibilities of a fixed point on the Poincare map.

For a fully actuated system, we have an additional degree of actuation, which gives us the possibility to improve the efficiency of the manipulation process. For example, we may minimize a cost function by proper design. Considering u_a as the additional actuator in the fully actuated system, we suppose that it has the form of:

$$u_a = f_u(\gamma, X), \tag{68}$$

in which, f_u is the general form that is to be determined, and X is a vector of coefficients relating u_a to γ. Also, let us consider:

$$J_u(X) = \frac{1}{T(\mathbf{x}_0)} \int_0^{T(\mathbf{x}_0)} \mathrm{PRI}(t)^2 dt, \tag{69}$$

which is a cost function to be minimized. Then, the optimization problem is defined as:

$$\min_X J_u(X) \qquad \text{subject to:}$$

$$c_{eq}(X) = 0, \qquad c(X) \le 0, \tag{70}$$

where $c_{eq}(X)$ and $c(X)$ are nonlinear (or even linear) functions containing constraints of the optimization problem. In addition, we may impose constraints onto PRI so that it must be in a given region. This way, the stability analysis of the system is as described before.

4. Results and simulation

To check our approach, we use three different examples. One example deals with a fully actuated manipulation system, while the two others are under-actuated. In the first example, we use single link, actuated manipulators to manipulate a multibody active object. The object has a body and two actuated arms. In the second example, we change the structure of the individual manipulators by adding another passive link to them. Therefore, each manipulator has two links one of which is passively jointed to the ground and the other is jointed to the first link while actuated. In the third example, we change the object to a two-link passive one. In addition, we add an actuator to the base of the manipulators used in the second example. Now, we apply our approach to undertake these manipulation processes.

4.1. Example 1: Dynamic manipulation of active objects using active manipulators

In this example, we use a simple 1-DoF active manipulator to manipulate a three-segment active object. The manipulator is a single link attached to the ground (Figure 1(c)) and has an actuator in the base, while the object has a body with two arms (Figure 1(a)) each of which is actuated by an independent actuator that is mounted on the body. Therefore, the integrated manipulator/object system is a fully actuated system

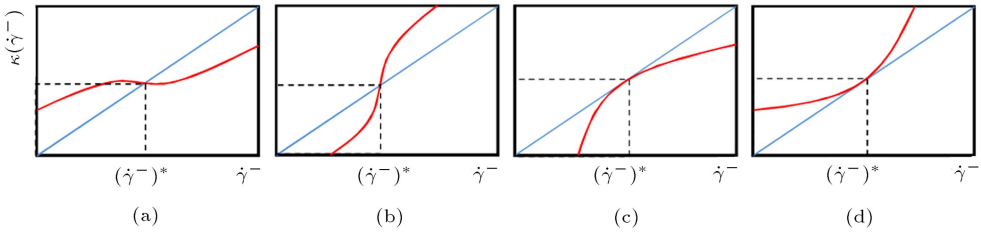

Figure 3. Four possibilities of a fixed point in the Poincare map: (a) Stable fixed point: The slope of the diagram is less than 1 in the fixed point; (b) unstable fixed point: The slope of the diagram is more than 1 in the fixed point; (c and d) semi stable fixed point: The slope of the diagram is 1 in the fixed point.

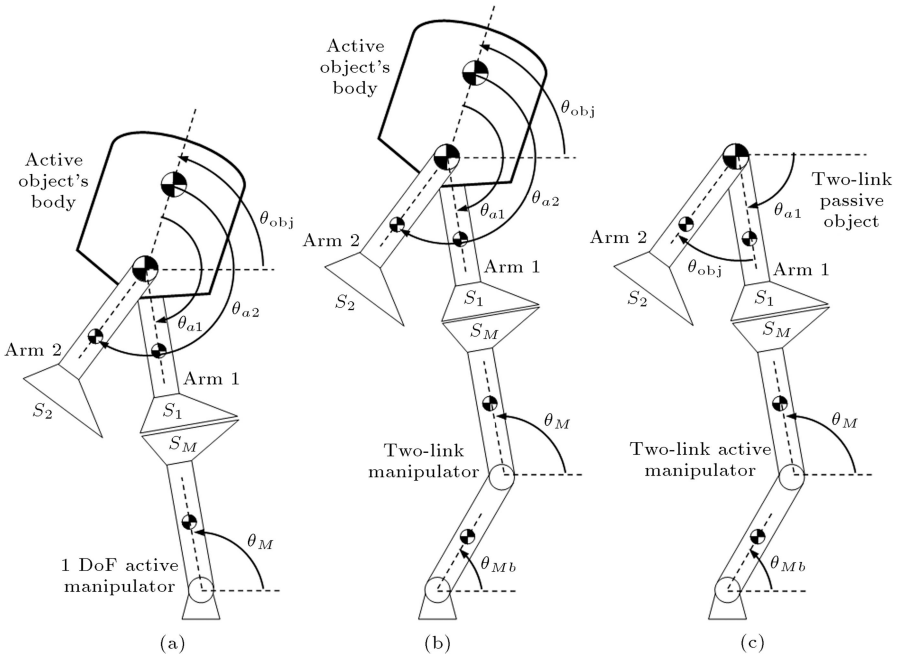

Figure 4. Three demonstrative models of manipulator/object and the corresponding joint coordinates: (a) Manipulation of a three-segment active object using a 1-link active manipulator; (b) manipulation of a three-segment active object using a 2-link under-actuated manipulator; and (c) manipulation of a two-link passive object using a 2-link active manipulator.

Table 1. Parameters corresponding to object and manipulators in Example 1.

Object		Manipulator	
L_A	0.25 m	L_M	0.5 m
L_a	0.125 m	L_m	0.25 m
L_O	0.2 m	M_m	3 kg
s	0.1 m		
a	0.025 m		
b	0.075 m		
m	1 kg		
M_j	2 kg		
M_O	2 kg		

(see Figure 4(a)). For simplicity, we assume that the object's body and arms have point mass at their center of mass without any distributed mass. In addition, we consider a point mass in the joint of the object's body and arms. Both arms of the object are similar, with the same parameters (see Figure 1(a)). The parameters for this example are as in Table 1.

For the generalized coordinates in the contact phase, we used a set of coordinates as:

$$\mathbf{q} = [q_1, q_2, q_3]^T. \tag{71}$$

And, for the impact phase, we chose:

$$\mathbf{q}_i = \left[\mathbf{q}^T, L_m \sin q_1, L_m \cos q_1\right]^T, \tag{72}$$

where (see Figure 4(a)):

$$q_3 = \frac{\pi}{2} - \theta_{\text{obj}}, \qquad q_1 = \frac{\pi}{2} - \theta_M = \pi - \theta_{a1} - q_3,$$
$$q_2 = \pi - \theta_{a2} - q_3. \tag{73}$$

To design a feedback control, we defined two outputs in the form of Eq. (66) and used these outputs to design appropriate control torques for the object's actuators. First, we defined $\gamma(\mathbf{q})$ in Eq. (66) as:

$$\gamma(\mathbf{q}) = q_1. \tag{74}$$

Then, we designed h_a and $h_d(\gamma)$ in Eq. (66) as:

$$h_a(\mathbf{q}) = \begin{bmatrix} q_3 \\ q_2 \end{bmatrix}, \tag{75}$$

$$h_d(\gamma(\mathbf{q})) = \begin{bmatrix} \frac{\pi}{9} \\ -q_1 \end{bmatrix}, \tag{76}$$

yielding:

$$\mathbf{y} = \begin{bmatrix} y_1 \\ y_2 \end{bmatrix} = \begin{bmatrix} q_3 - \frac{\pi}{9} \\ q_1 + q_2 \end{bmatrix}. \tag{77}$$

Zeroing these outputs, the controller forces the object's body to have an angle of $\pi/9$ and arm 2 to have a mirror position of arm 1 with respect to the vertical axis. Then, Eq. (64) will be as:

$$\psi\left(\mathbf{y}, \dot{\mathbf{y}}, \alpha_1, \alpha_2\right) = \frac{1}{\varepsilon^2}\begin{bmatrix} k_1\left(-|y_1|^{\alpha_1}\operatorname{sign}(y_1) - |\varepsilon\dot{y}_1|^{\alpha_2}\operatorname{sign}\left(\varepsilon\dot{y}_1\right)\right) \\ k_2\left(-|y_2|^{\alpha_1}\operatorname{sign}(y_2) - |\varepsilon\dot{y}_2|^{\alpha_2}\operatorname{sign}\left(\varepsilon\dot{y}_2\right)\right) \end{bmatrix}, \tag{78}$$

Table 2. Adjusted controller parameters for Example 1.

α_1	0.85
α_2	0.9
ε	0.8
k_1	1
k_2	1

where $\varepsilon > 0$ determines the settling time of the controller The adjusted parameters used for the controller, are as in Table 2.

To design the control torque of the manipulator's actuator, we started from Eq. (68) and considered u_a, the torque of the manipulator's actuator, as a 3rd degree polynomial function of γ that is:

$$u_a = f_u(\gamma, X) = a_0 + a_1 q_1 + a_2 q_1^2 + a_3 q_1^3, \tag{79}$$

where:

$$X = [a_0, a_1, a_2, a_3]^T, \tag{80}$$

is the vector of coefficients. This vector was also used as the vector of variables in the optimization problem (70). Then, we used a Genetic Algorithm (GA) to minimize the cost function (69) under Constraints (46) to (50). In addition, we forced the Poincare map (67) to have a fixed point of 1.2 by adding a penalty term to the cost function. The GA was terminated after 60 iterations; the results are listed in Table 3.

Using Eq. (74), we construct the Poincare map, κ, in Eq. (67) as:

$$\dot{q}_1^-|_{k+1} = \kappa\left(\dot{q}_1^-|_k\right). \tag{81}$$

Table 3. GA setting and results in Example 1.

Method	GA
Iteration	60
Population size	20
Best fitness	0.0836
Mean fitness	0.1222
a_0	2.2569
a_1	-6.9504
a_2	2.6602
a_3	-1.2740

For any given q_1^- and $\dot{q}_1^-$, say $\dot{q}_1^-|_k$, if the controller forces output y to zero, we have:

$$q_2^- = -q_1^-, \qquad q_3^- = \frac{\pi}{9}, \qquad \dot{q}_2^- = -\dot{q}_1^-, \qquad \dot{q}_3^- = 0. \tag{82}$$

Then, we may apply Eq. (57) to $\mathbf{x}^-$ to compute $\mathbf{x}^+$. Solving Eq. (58) with $\mathbf{x}^+$ as its initial conditions, gives us the next $\dot{q}_1^-$, namely, $\dot{q}_1^-|_{k+1}$. Figure 5 shows the Poincare map and phase diagrams of generalized coordinates in this example. It depicts the variation of Poincare function κ for $\dot{\gamma}^- \in [1.1, 1.3]$ rad/s when $\gamma^- = \pi/12$ rad. In the Poincare diagram, the dashed line is the identity function to show the slope of the Poincare diagram at the fixed point, $\dot{\gamma}^- \cong 1.217$ rad/s. It is clear that the slope of the diagram is less than 1 and, therefore, the fixed point is stable. The straight lines in the phase diagrams correspond to impact occurrence. Furthermore, these diagrams include dashed curves that represent the limit cycles of general coordinates.

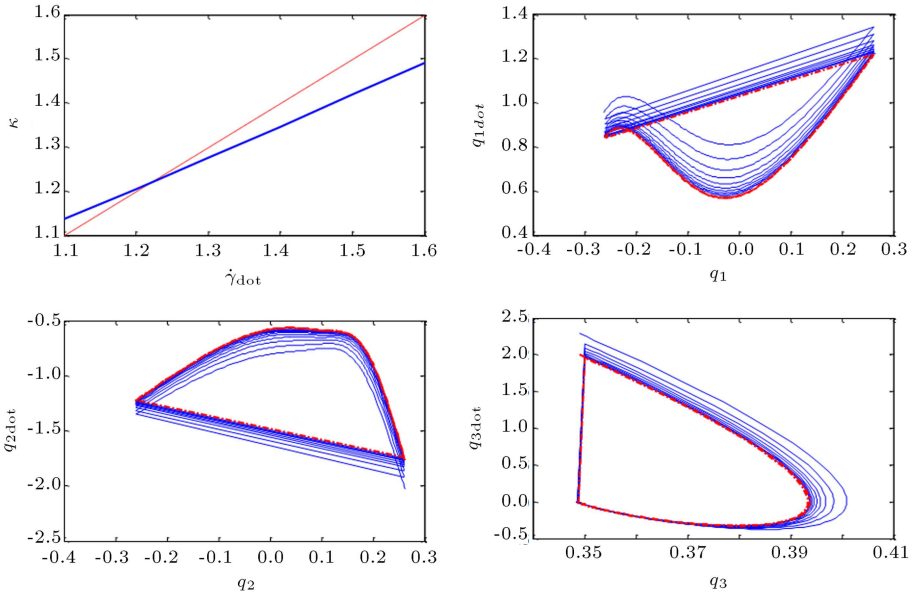

Figure 5. Poincare map and phase diagram of generalized coordinates in Example 1. Poincare map: Solid line is the Poincare map; dashed line is the identity function. Phase diagrams: Solid lines are the phase diagrams and dash-dotted lines are the limit cycles of the coordinates.

Outputs of the system defined in Eq. (77) are shown in Figure 6. As expected, they become zero before impact occurrence. Figure 7 shows the control actions of the actuators of both manipulator and object. It is notable that τ_b, corresponding to the manipulator base, is a 3rd degree polynomial function of γ with optimized coefficients listed in Table 3.

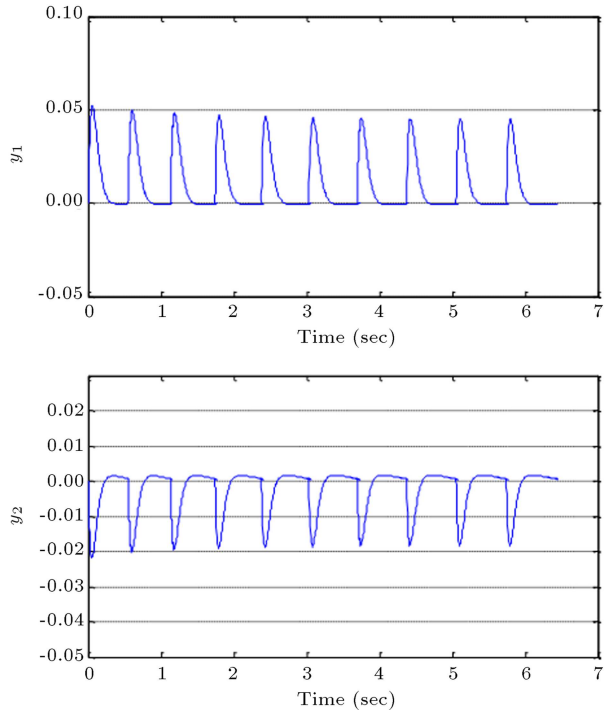

Figure 6. Outputs variation of the system (Example 1).

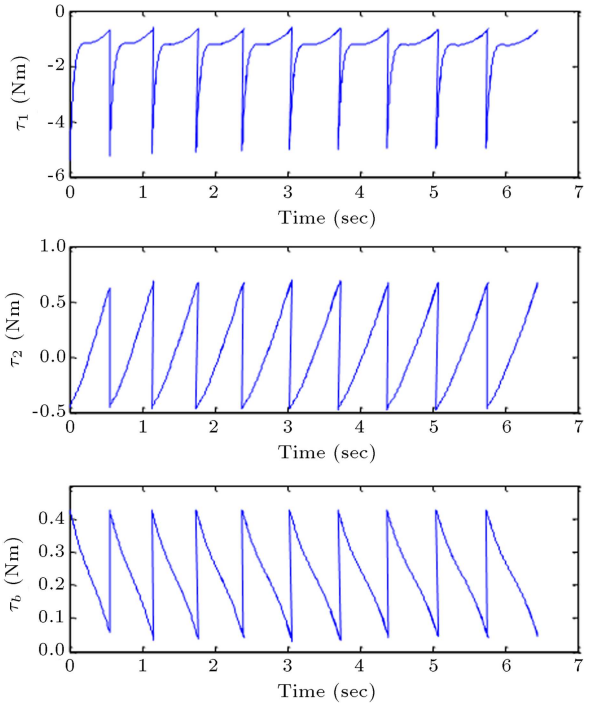

Figure 7. Control actions of the system (Example 1).

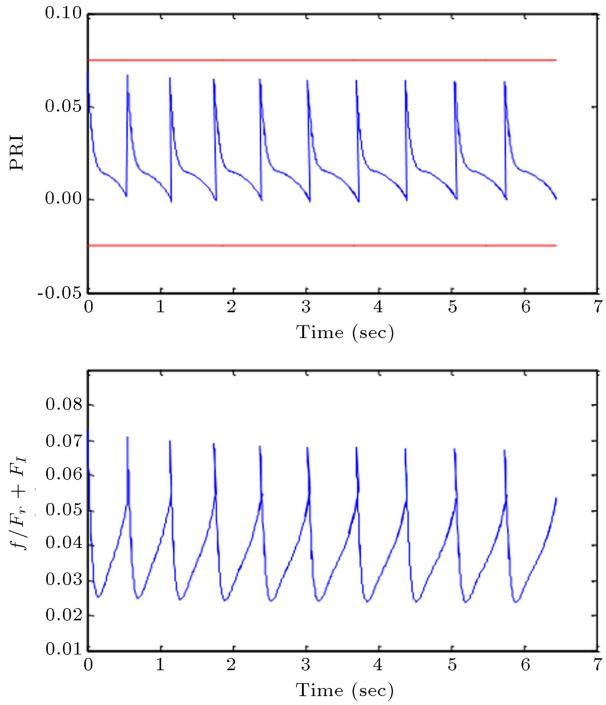

Figure 8. PRI variation and its margins, and friction force divided by total normal force in contact surface of the object (Example 1).

In Figure 8, we see the diagrams of PRI variation and frictional force divided by normal force on the contact surface during the contact phase. Two lower and upper bounds representing the edges of the object's contact surface, however, surround the PRI diagram. Therefore, we conclude that PRI remains in bounds and the object does not rotate with respect to the contacting manipulator. The other diagram shows that no slip occurs for small values of the frictional coefficient, e.g. $\mu > 0.08$.

4.2. Example 2: Dynamic manipulation of active objects using under-actuated manipulators

In this example, we use a two-link manipulator to manipulate a three-segment active object. The object is the same as that in the previous example. However, the manipulators have some differences. In fact, we have added a passive link to the manipulator in Example 1 (see Figure 1(d) for details). In this example, each manipulator is passively jointed to the ground and a second link is attached to the first link while actuated by an actuator mounted on the first link. Therefore, the integrated manipulator/object system is an under-actuated actuated system (see Figure 4(b)). The mass distribution is as in the previous example (see Figure 1(b)). The parameters for this example are as in Table 4.

In this example, we used absolute angles to define generalized coordinates. Therefore, for the generalized

Table 4. Parameters corresponding to object and manipulators in Example 2.

Object		Manipulator	
L_A	0.5 m	L_M	0.5 m
L_a	0.25 m	L_m	0.25 m
L_O	0.5 m	M_m	3 kg
s	0.1 m	L_{Mb}	0.5 m
a	0.05 m	L_{mb}	0.25 m
b	0.05 m	M_{mb}	0.5 kg
m	0.5 kg		
M_j	2 kg		
M_O	0.5 kg		

coordinates in the contact phase, we used a set of coordinates as:

$$\mathbf{q} = [q_1, q_2, q_3, q_4]^T, \tag{83}$$

and for the impact phase, we chose:

$$\mathbf{q}_i = [\mathbf{q}^T, L_m \cos q_1 + L_{Mb} \cos q_4, L_m \sin q_1 + L_{Mb} \sin q_4]^T, \tag{84}$$

where (see Figure 4(b)):

$$q_1 = \theta_M, \qquad q_2 = \theta_{a2} + \theta_{\text{obj}},$$
$$q_3 = \theta_{\text{obj}}, \qquad q_4 = \theta_{Mb}. \tag{85}$$

Again, we defined three outputs to design a feedback control. Thus, we defined $\gamma(\mathbf{q})$ in Eq. (66) as:

$$\gamma(\mathbf{q}) = L_M \cos q_1 + L_{Mb} \cos q_4, \tag{86}$$

which is, in fact, the horizontal displacement of the object' actuators. Then we designed h_a and $h_d(\gamma)$ in Eq. (66) so that the outputs became:

$$\mathbf{y} = \begin{bmatrix} y_1 \\ y_2 \\ y_3 \end{bmatrix} = \begin{bmatrix} q_3 - \frac{\pi}{2} + \frac{\pi}{12} \\ q_1 - q_4 + k_{\text{bios}}\gamma \\ q_2 + q_4 - k_{\text{bios}}\gamma - \pi \end{bmatrix}. \tag{87}$$

Zeroing these outputs, the controller forces the object's body to have an angle of $\pi/12$, and arm 2 to have a mirror position of arm 1, with respect to the vertical axis. Moreover, the base of the manipulator has a bios angle, with respect to the end-effector, which is a function of the horizontal displacement of the object, adjusted using an adjusting gain, k_{bios}. The adjusted parameters of the controller (64) are listed in Table 5.

In this example, $\dot{\gamma}$ in Poincare map κ, as introduced by Eq. (67), is the horizontal velocity of the object. Any horizontal displacement and velocity of the object, γ and $\dot{\gamma}$, may be applied to Eqs. (86) and (87) to derive $\mathbf{q}^-$ and $\dot{\mathbf{q}}^-$ when $\mathbf{y} \equiv 0$. Again, applying Eq. (57) to $\mathbf{x}^-$ gives us $\mathbf{x}^+$. Solving Eq. (58), with $\mathbf{x}^+$ as its initial conditions, results in the next $\dot{q}_1^-$, namely, $\dot{q}_1^-|_{k+1}$.

Table 5. Adjusted controller parameters for the Example 2.

α_1	0.85
α_2	0.9
ε	0.1
k_1	1
k_2	1
k_{bios}	0.4

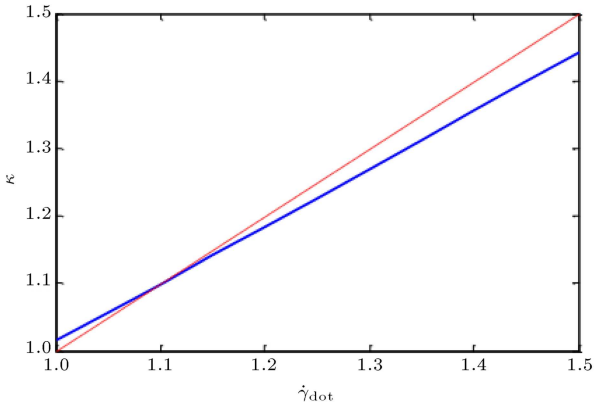

Figure 9. Poincare map of Example 2.

The Poincare map in this example can be seen in Figure 9. The Poincare diagram is plotted for $\dot{\gamma}^- \in [1, 1.5]$ m/s, when $\gamma^- = 0.35$ m. In the Poincare diagram, the dashed line is the identity function to show the slope at the fixed point, $\dot{\gamma}^- \cong 1.093$ m/s. The slope of the diagram is less than 1 at the fixed point and, therefore, the fixed point is stable. Figure 10 shows the phase diagrams of generalized coordinates. These diagrams are evidently stable and tend to their limit cycles plotted in dashed lines. In addition, outputs of the system are shown in Figure 11. As expected, they become zero before impact occurrence. Figure 12 illustrates the control actions of the actuators of both manipulator and object. In Figure 13, we may see the diagrams of PRI variation and frictional force divided by normal force on the contact surface during the contact phase. Two lower and upper bounds, representing the edges of the object's contact surface, however, surround the PRI diagram. Again, we conclude that PRI remains in bounds and the object does not rotate with respect to the contacting manipulator. The other diagram in this figure tells us no slip occurs for ordinary values of the frictional coefficient, e.g. $\mu > 0.4$.

4.3. Example 3: Dynamic manipulation of passive objects using fully actuated manipulators

Here, we add an actuator to the passive joint of the individual manipulators as in the previous example. For

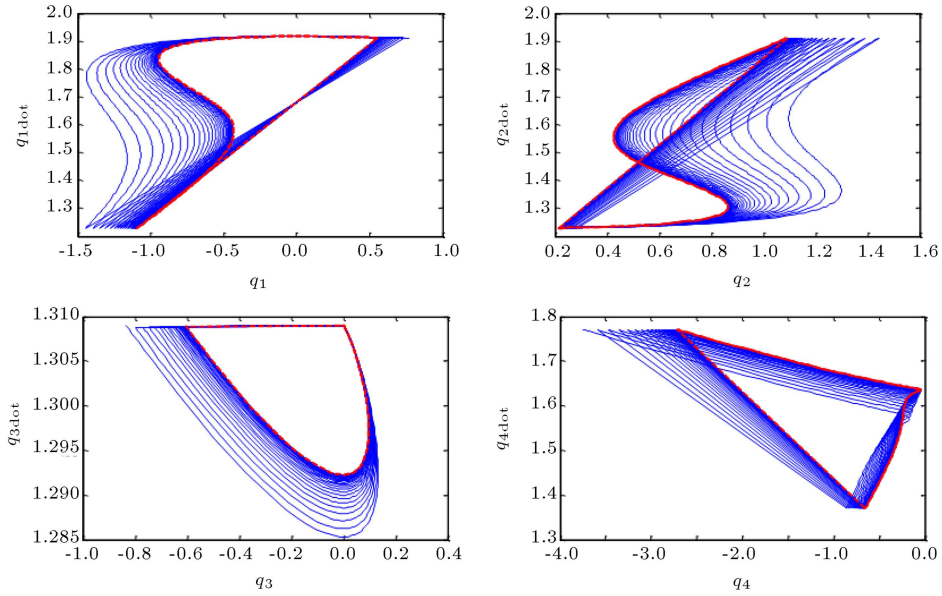

Figure 10. Phase diagram of generalized coordinates in Example 2.

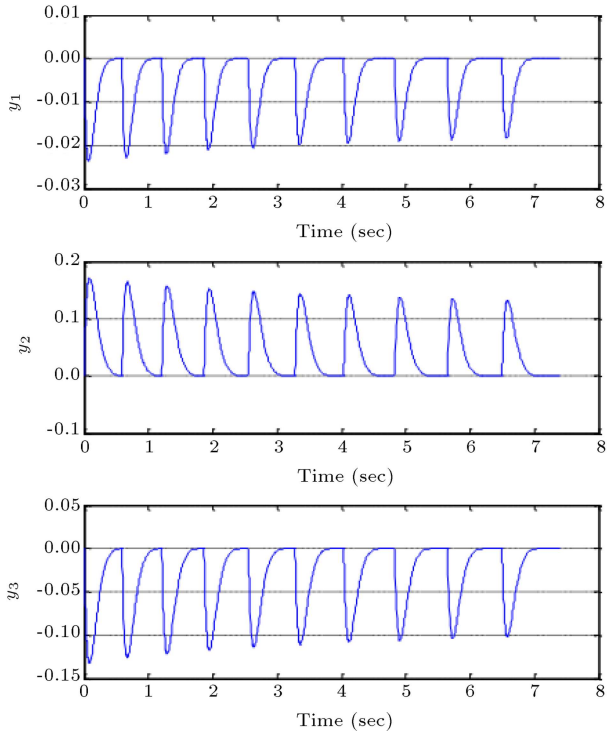

Figure 11. Outputs of Example 2.

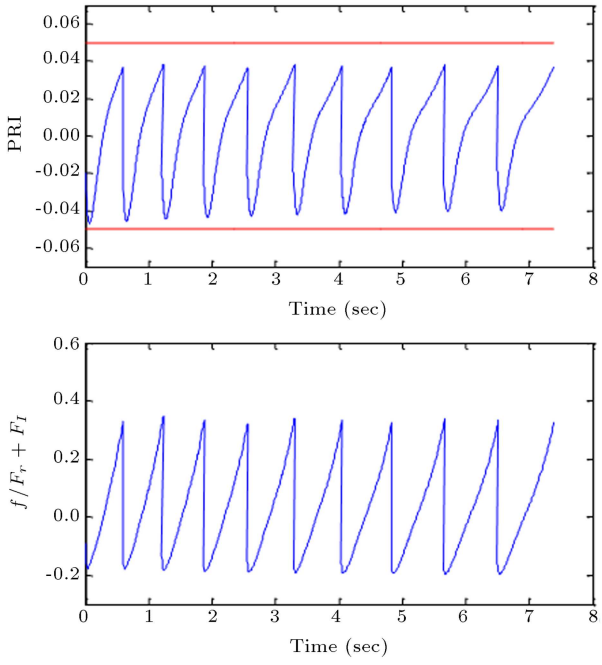

Figure 12. Inputs of Example 2.

the object, we use a two-link passive model illustrated in Figure 1(b). The parameters for this example are in Table 6.

For the generalized coordinates in both contact and impact phases, $\mathbf{q} = [q_1, q_2, q_3]^T$ and $\mathbf{q}_i$, we used a set of coordinates as (Figure 4(c)):

$$q_1 = \theta_M, \qquad q_2 = \theta_M + \theta_{\text{obj}} - \pi,$$
$$q_3 = \theta_{Mb}, \tag{88}$$

$$\mathbf{q}_i = \left[\mathbf{q}^T, L_{Mb}\cos q_3 + L_M \cos q_1, L_{Mb}\sin q_3 + L_M \sin q_1\right]^T. \tag{89}$$

We chose:

$$\gamma(\mathbf{q}) = q_2, \tag{90}$$

$$h_d(\gamma) = -\begin{bmatrix} \gamma \\ (k_{\text{bios}}+1)\gamma + k_{\text{bios}}\frac{\pi}{2} \end{bmatrix}, \tag{91}$$

$$h_a(q) = \begin{bmatrix} q_1 \\ q_3 \end{bmatrix}. \tag{92}$$

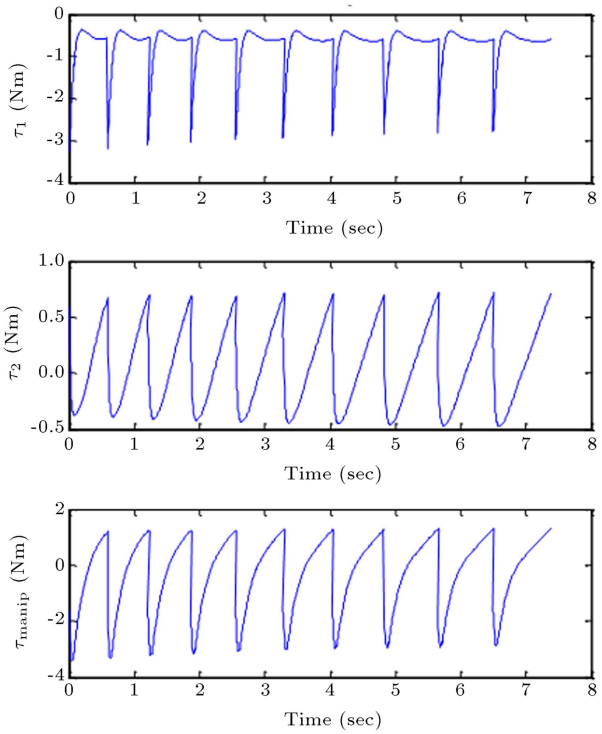

Figure 13. PRI diagram; tangential force divided by normal force in contact surface.

Table 6. Parameters corresponding to object and manipulators in Example 3.

Object		Manipulator	
L_A	0.25 m	L_M	0.2 m
L_a	0.125 m	L_m	0.1 m
L_O	0.2 m	M_m	0.1 kg
s	0.2 m	L_{mb}	0.3 m
a	0.1 m	L_{mb}	0.15 m
b	0.1 m	M_{mb}	0.1 kg
m	0.1 kg		
M_j	2 kg		

Table 7. Adjusted controller parameters for Example 3.

α_1	0.99
α_2	0.99
ε	0.08
k_1	1
k_2	1
k_{bios}	0.3

In addition, we adjusted the controller parameters as listed in Table 7. The selection and analysis of the Poincare map is straightforward and similar to the two previous examples. In Figure 14, κ has been shown for $q_2^- = -\pi/2.3$ rad and $\dot{q}_1^- \in [0.05, 0.95]$. It is seen that there exists a fixed point at $\dot{q}_1^- \cong 0.206$ rad/s. Since the slope of the diagram is less than one at the fixed point, it is an asymptotically stable fixed point of the system. Limit cycles associated with this fixed point and phase diagram of the system's states for initial condition $\dot{q}_1^- = 0.3$ rad/s are depicted in Figure 14, as well. Figure 15 depicts the evolution of outputs during ten cycles of the manipulation process, while Figure 16 shows the diagram of control torques of the system's actuators. Finally, Figure 17 illustrates the variation of the PRI

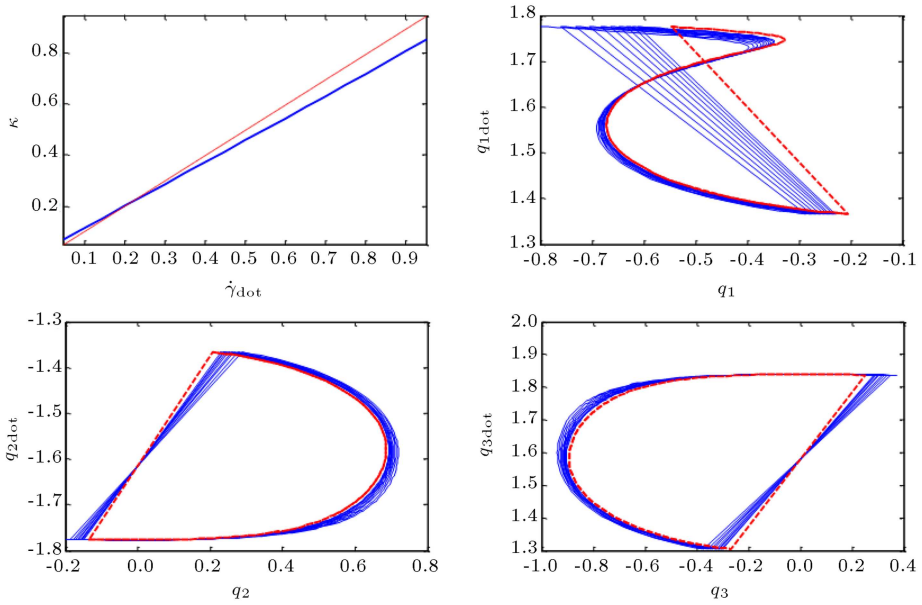

Figure 14. Poincare map and phase diagram of generalized coordinates in Example 3. Poincare map: Solid line is the Poincare map; dashed line is the identity function. Phase diagrams: Solid lines are the phase diagrams and dash-dotted lines are the limit cycles of the coordinates.

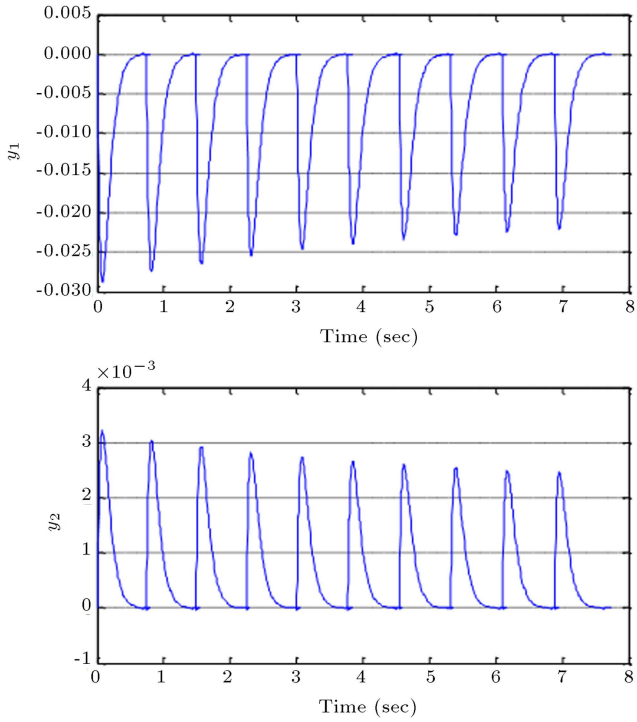

Figure 15. Output variations of the system in Example 3.

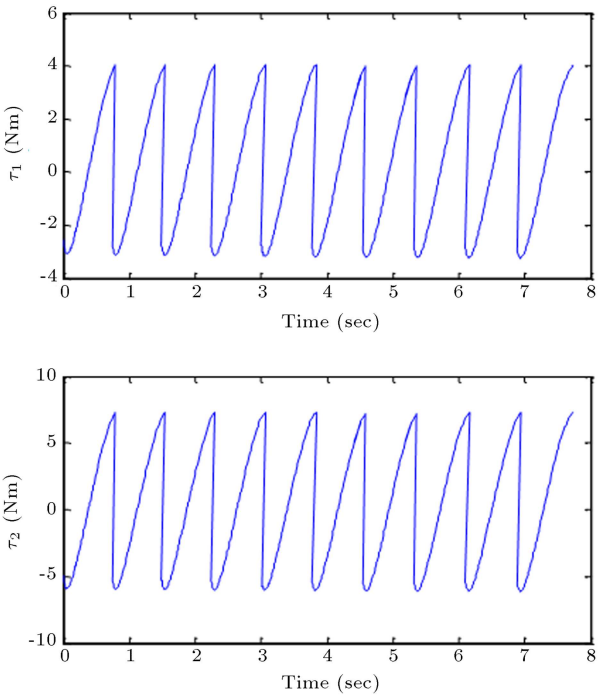

Figure 16. Control actions of the system (manipulators) in Example 3.

point during the manipulation process in the current example. Moreover, the diagram of tangential force divided by normal force in the contact surface is included in this figure. It is evident that for small values of μ_s, e.g. $\mu_s > 0.15$, there is no slip in the contact surface.

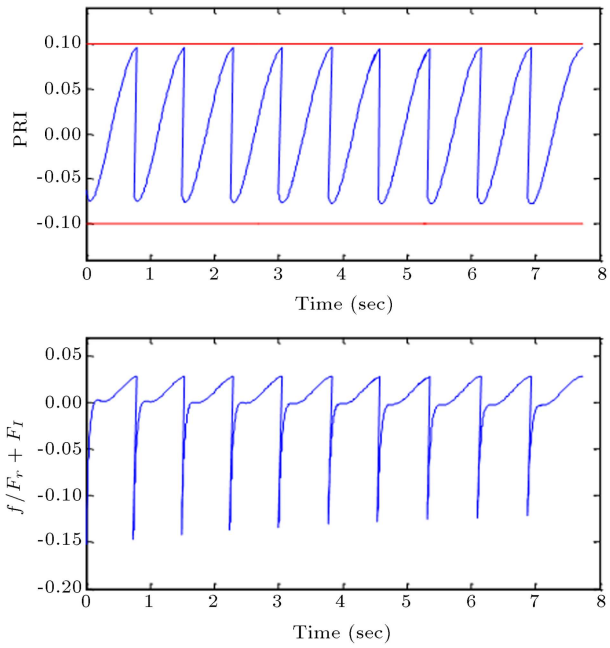

Figure 17. PRI variation and its margins, and friction force divided by total normal force in the contact surface of the object in Example 3.

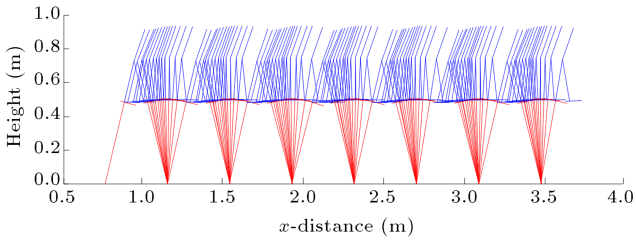

Figure 18. Some snapshots of the manipulation process corresponding to Example 1.

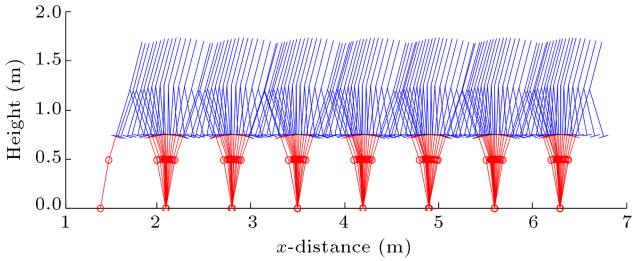

Figure 19. Some snapshots of the manipulation process corresponding to Example 2.

5. Discussion

According to the results obtained, it is obvious that our approach to handling the dynamic manipulation process in three different cases is successful; some snapshots of the processes are indicated in Figures 18 to 20. However, the main concerns regarding the systems studied are control strategies, which must be applied to control them. In particular, underactuated systems need more attention because of one degree

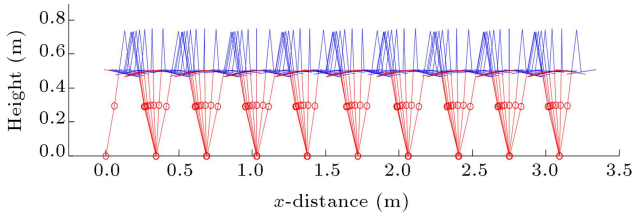

Figure 20. Some snapshots of the manipulation process corresponding to Example 3.

of underactuation, which leads to them not being completely controlled. The Poincare map of Example 1 shows a wider domain of stability in comparison to those of Examples 2 and 3, which include some passivity in the structure of either object or manipulator. In these underactuated systems (Examples 2 and 3), other control methods that have been applied to underactuated systems (like point feet walkers) in the literature, could be helpful as well.

6. Conclusion and future works

In this paper, we dealt with a special kind of manipulation, during which, a multibody object was manipulated by a series of manipulators. We define the general problem and note that it is nonlinear with impulse effects. We categorized the whole process and divided it into separate cycles. Then, each cycle was divided into two phases, i.e. contact and impact phases. For each phase, an appropriate model and formulation were derived. By making some modifications to previous approaches described in the literature of dynamical systems with impulse effects, the problem was successfully solved. We use PRI points to check if the object would rotate, with respect to the manipulators, during the manipulation process. In addition, sufficient conditions were derived under which no slippage would occur during manipulation or in the impact phase. An asymptotical stability study of the system was proposed using the analysis of the Poincare map.

To check the validity of the approach, we define and solve three examples. In these examples, both active and passive objects, and both passive and active manipulators, are used to manipulate the objects. The orbital stability of the manipulation in each example was proved.

Nomenclature

S_M^k	Contact surface of manipulator, k
S_i	Contact surface of object's arm, i, $(i = 1, 2)$
τ_k	Time of impact, k
$\mathbf{M}$	Mass matrix
$\mathbf{q}$	Generalized coordinates of the contact phase
$\mathbf{x}$	State variable in contact phase
$\mathbf{x}_0$	Initial state
$\mathbf{C}$	Bios matrix
$\mathbf{G}$	Vector of gravitational effects
$\mathbf{B}$	Matrix of distribution $\mathbf{u}$ among generalized coordinates
$\mathbf{u}$	Vector of the torques of the system's actuators
$\mathbf{y}$	Vector of the outputs of the system
h	Output function of the system
$\mathbf{P}_O^{\mathrm{CM}}$	Position vector of the object's center of mass
ψ	Position function of $\mathbf{P}_O^{\mathrm{CM}}$
$\mathbf{v}_O^{\mathrm{CM}}$	Velocity vector of the object's center of mass
$\mathbf{a}_O^{\mathrm{CM}}$	Acceleration vector of the object's center of mass
F_c^i	Force vector acting on contact surface, S_i $(i = 1, 2)$ in P_s^i
m_{total}	Total mass of object
$\mathbf{R}$	Rotational matrix
g	Vector of gravity
P_s^i	Intersection of S_i and the line from the last joint of manipulator k to the first joint of arm i $(i = 1, 2)$
$\mathbf{P}_s^i$	Position vector of P_s^i
M_c^i	Moment vector acting on contact surface, S_i $(i = 1, 2)$
$\mathbf{H}$	Total object's angular momentum about its center of mass
F_l, F_r	Normal forces acting on left and right edges of S_1 due to normal element of F_c^1
f	Tangential element of F_c^1 acting on S_1
$\mathbf{e}_k$	Unit vector of direction, k, $\left(k = x, y, z, \bar{x}, \bar{y}, \bar{z}, X, Y, Z, \bar{X}, \bar{Y}, \bar{Z}\right)$
a, b	Distances of left and right edges of S_i $(i = 1, 2)$ from P_s^i
μ_s	Coefficient of static friction
PRI	Palm Rotation Indicator
d_{PRI}	Distance of PRI from P_s^i $(i = 1, 2)$
q_i	Generalized coordinates in impact phase
$\mathbf{J}$	Jacobean matrix of mapping $\mathbf{F}_{\mathrm{ext}}$ of $\mathbf{q}$
$\mathbf{F}_{\mathrm{ext}}$	External forces at the base of manipulator $k + 1$

$\hat{\mathbf{F}}_{\text{ext}}$	External impulse forces at the base of manipulator $k+1$
$\bar{\Delta}_P, \bar{\Delta}_V$	Pre-transition functions mapping generalized coordinates and velocities of contact phase and those of impact phase just before impact
Δ_P, Δ_V	Transition functions mapping generalized coordinates and velocities before impact in the impact phase, and those of the next contact phase
ϵ	Restitution coefficient
$(V_s^i)_k$	Image of velocity vector of P_s^i $(i=1,2)$ on direction k $\left(k=x,y,z,\bar{x},\bar{y},\bar{z},X,Y,Z,\bar{X},\bar{Y},\bar{Z}\right)$
$(V_M^k)_k$	Image of velocity vector of a point on end effector k, coinciding with P_s^i $(i=1,2)$ on direction k $\left(k=x,y,z,\bar{x},\bar{y},\bar{z},X,Y,Z,\bar{X},\bar{Y},\bar{Z}\right)$
θ_s^i	Orientation of contact surface, S_i $(i=1,2)$
θ_M^k	Orientation of contact surface, S_M^k
$\Delta V_{S_1/S_M}$	Relative velocity of P_s^i $(i=1,2)$ with respect to its corresponding point on S_M^k in the y direction
$\mathbf{\Sigma}$	Momentum of the system
$\mathbf{\Sigma}_{\text{before}}$	Momentum of the system just before impact
$\mathbf{\Sigma}_{\text{after}}$	Momentum of the system just after impact
$\mathbf{M}_{S_M}$	Mass matrix corresponding to the end effector of the manipulator, $k+1$
K_{S_M}	Kinetic energy corresponding to the end effector of the manipulator, $k+1$
S	Impact hyper surface
E	Any function of $\mathbf{q}$, the vanishing of which indicates the reaching of arm 1 to end-effector $k+1$
$\mathcal{L}$	Lie operator
v	Control action
α_1, α_2	Controller parameters
h_a	A part of h following a desired trajectory
h_d	A part of h that should be designed and followed by h_a
γ	Function of generalized coordinates, $\mathbf{q}$
κ	Poincare map
u_a	Action of base actuator that should be optimized
f_u	General form of u_a as a function of X
X	Variable vector of optimization problem
J_u	Cost function of optimization problem
$T(x_0)$	Duration of each cycle of manipulation as a function of initial state x_0
$c_{eq}(X)$	Equality constraints of the optimization problem
$c(X)$	Inequality constraints of the optimization problem
L_A	Length of object's arm
L_a	Distance of arm's center of mass from its joint
L_O	Distance of center of mass of object's body from arm's joint
s	Length of contact surface of object
m	Mass of each leg of object
M_j	Mass of object concentrated in arm's joint
M_O	Mass of object's body
L_M	Length of manipulator's end effector
L_m	Distance of center of mass of manipulator's end effector from its joint
L_{Mb}	Length of manipulator's base link
L_{mb}	Distance of center of mass of manipulator's base link from its base
M_m	Mass of manipulator's end effector
M_{mb}	Mass of manipulator's base link
θ_{obj}	Orientation of object
θ_{a1}, θ_{a2}	Orientation of arms 1 and 2 of the object
θ_M, θ_{Mb}	Orientation of end effector and base link of manipulator
ψ	Controller function
ε	Adjusting parameter of controller
k_1, k_2	Gains of controller
sign	Sign function
a_k	Polynomial coefficients of mapping u_b to γ
τ_b	Actuator torque corresponding to u_b
k_{bios}	Adjusting parameter of manipulator configuration
$\dot{\square}, \ddot{\square}$	First and second time-derivative of a variable
$\hat{\square}, \bar{\square}$	Impulse vectors and functions in impact phase corresponding to those in contact phase
$\square^+, \square^-$	Any parameter referring to just after and just before impact

References

1. Lynch, K.M. and Black, C.K. "Recurrence, controllability, and stabilization of juggling", *IEEE Trans. on Rob. Aut.*, **17**(2), pp. 113-124 (2001).
2. Beigzadeh, B., AhmadAbadi, M.N. and Meghdari, A. "Dynamic object manipulation (DOM) of a sphere using two manipulators", *IEEE Int. Conf. on Mechat. Aut.*, China, pp. 1191-1196 (2006).
3. Beigzadeh, B., Meghdari, A. and Beigzadeh, Y. "Dynamic manipulation of objects using a series of manipulators", *Proc. of ASME Int. Mech. Eng. Cong. and Exp.*, Seattle, USA (2007).
4. Akbarimajd, A., Ahmadabadi, M.N. and Beigzadeh, B. "Dynamic manipulation by an array of 1 DOF manipulators: Kinematical modeling and planning", *Rob. and Auton. Sys.*, **55**, pp. 444-459 (2007).
5. Lynch, K.M. and Mason, M.T. "Dynamic manipulation with a one joint robot", *IEEE Int. Conf. on Rob. and Aut.*, **1**, pp. 359-366 (1997).
6. Lynch, K.M. and Mason, M.T. "Stable pushing: Mechanics, controllability, and planning", *Int. J. Rob. Res.*, **15**(6), pp. 533-556 (1996).
7. Akella, S., Huang, W., Lynch, K.M. and Mason, M.T. "Parts feeding on a conveyor with a one joint robot", *Algorithmica*, **26**(3), pp. 313-344 (2000).
8. Makarem, L., Akbarimajd, A. and Ahmadabadi, M.N. "Dynamic manipulation of active objects: Modeling and optimization", *IEEE/ASME Int. Conf. on Adv. Intel. Mechat.*, pp. 1400-1405 (2009).
9. Beigzadeh, B., Meghdari, A. and Sohrabpour, S. "Control and manipulation of multibody objects", *ASME 10 Bien. Conf. on Eng. Sys. Des. and Anal.*, pp. 579-584 (2010).
10. Beigzadeh, B., Meghdari, A. and Sohrabpour, S. "Manipulation of multibody active objects using simple passive manipulators", *ASME Int. Mech. Eng. Cong. and Exp.*, pp. 597-603 (2010).
11. Beigzadeh, B., Meghdari, A. and Sohrabpour, S. "Passive dynamic object manipulation: Preliminary definition and examples", *Act. Aut. Sin.*, **36**(12), pp. 1711-1719 (2010).
12. Beigzadeh, B., Meghdari, A. and Sohrabpour, S. "Passive dynamic object manipulation: A framework for passive walking systems", *Proc. of Ins. of Mech. Eng., Part K: J. of Mul.-bod. Dyn.*, **227**(2), pp. 185-198 (2013).
13. Tedrake, R., Weirui Zhang, T., Fong, M. and Sebastian Seung, H. "Actuating a simple 3D passive dynamic walker", *Proc. of IEEE Int. Conf. on Rob. and Aut.*, **5**, pp. 4656-4661 (2004).
14. Sabaapour, M.R., Hairi-Yazdi, M.R. and Beigzadeh, B. "Towards passive turning in biped walkers", *Proc. Tech.*, **12**, pp. 98-104 (2014).
15. Bainov, D.D. and Simeonov, P.S., *System with Impulse Effects: Stability, Theory and Applications*, Ellis Horwood, Chichester (1989).
16. Hurmuzlu, Y. and Moskowitz, G.D. "Bipedal locomotion by impact and swithing: I. Two- and three-dimensional, three-element models", *Dyn. and Stab. of Sys.*, **2**(2), pp. 75-96 (1987).
17. Hurmuzlu, Y. and Moskowitz, G.D. "Bipedal locomotion by impact and swithing: II. Structural stability analysis of a four-element bipedal locomotion model", *Dyn. and Stab. of Sys.*, **2**(2), pp. 97-112 (1987).
18. Grizzle, J.W., Abba, G. and Plestan, F. "Asymptotically stable walking for biped robots: Analysis via systems with impulse effects", *IEEE Trans. on Aut. Cont.*, **46**, pp. 51-64 (2001).
19. Grizzle, J.W., Abba, G. and Plestan, F. "Proving asymptotic stability of a system of a walking cycle for a 5 DOF biped robot model", *Proc. of Int. Conf. on Climb. and Walk. Rob.*, England (1999).
20. Beigzadeh, B., Meghdari, A. and Beigzadeh, Y. "Dealing with biped locomotion as a dynamic object manipulation problem: Manipulation of body using legs", *Proc. of ASME Int. Mech. Eng. Cong. and Exp.*, Seattle, USA (2007).
21. Haimo, V. "Finite time controllers", *SIAM J. of Cont. and Opt.*, **24**(4), pp. 760-770 (1986).
22. Goswami, A. "Postural stability of biped robots and the Foot-Rotation Indicator (FRI) point", *Int. J. of Rob. Res.*, **18**(6), pp. 523-533 (1999).
23. Beigzadeh, B., Meghdari, A. and Sohrabpour, S. "PRI (Palm Rotation Indicator): A metric for postural stability in dynamic nonprehensile manipulation", *Mechanika*, **18**(4), pp. 461-466 (2012).
24. Hurmuzlu, Y. and Chang, T.H. "Rigid body collisions of a special class of planar kinematic chains", *IEEE Tran. on Sys. Man and Cyb.*, **22**(5), pp. 964-970 (1992).

Biographies

Borhan Beigzadeh received his PhD degree in Mechanical Engineering from Sharif University of Technology in 2011. His PhD thesis included work on dynamic walking systems and their correlation to dynamic passive/active manipulation systems. He then joined Iran University of Science and Technology (IUST) in Tehran, where he is currently Assistant Professor in the School of Mechanical Engineering. His research interests cover nonlinear dynamics and control, biomechatronics systems, cognitive sciences and traditional sciences.

Ali Meghdari received his PhD degree in Mechanical Engineering from the University of New Mexico, USA, in 1987. He then joined the robotics group of the Los Alamos National Laboratory (LANL) as a research collaborator. In 1988, he joined Sharif University of Technology (SUT), Tehran, Iran, and, in 1997, was recognized by the Iranian Society of Mechanical

Engineers as the youngest (at age 37) Mechanical Engineering full-Professor in Iran. From 1996 $\sim$ 1999, he also chaired the School of Mechanical Engineering at the University. From 1993 $\sim$ 1994, he was a visiting research student at the Advanced Highway Maintenance and Construction Technology (AHMCT) Centre at the University of California-Davis, USA, and, from 1999 $\sim$ 2000, worked at the Intelligent Biomedical Devices and Musculoskeletal Systems (IBDMS) Research Centre, Colorado School of Mines, and the Rocky Mountain Musculoskeletal Research Laboratory (RMMRL) as a visiting research professor.

His research interests cover robotics dynamics, flexible manipulators kinematics/dynamics, and dynamic modeling of biomechanical systems. He has published over 125 technical papers in refereed international journals and conferences, and has been the recipient of various scholarships and awards, the latest being the 2001 Mechanical Engineering Distinguished Professorship Award from Iran, and the 1997 Islamic Educational, Scientific and Cultural Organization (IESCO) Award in Technology from Morocco. He was also elected as a fellow of the American Society of Mechanical Engineers (ASME) in 2001, and has been member of the Academy of Sciences of I. R. Iran since 2004. From 2001-2010, he was the Vice-President of Academic Affairs at Sharif University of Technology, when he also played a key role in the establishment of SUT's International Campus on Kish Island, Iran. He was Founder and Director of the newly established Department of Languages and Linguistics in SUT from 2009-2012, and is currently the Director of the Center of Excellence in Design, Robotics and Automation (CEDRA), and Project Manager for SUT's new (under construction) Research & Technology Campus (RTC). He is on the editorial board of various engineering journals, and since 2005 has been an affiliate member of the Iranian Academy of Sciences (IAS).